

Plasma hydrodynamics of the intense laser-cluster interaction

H. M. Milchberg,¹ S. J. McNaught,^{1,2} and E. Parra¹

¹*Institute for Physical Science and Technology, University of Maryland, College Park, Maryland 20742*

²*National Institute of Standards and Technology, Gaithersburg, Maryland 20899*

(Received 23 May 2001; published 12 October 2001)

We present a one-dimensional hydrodynamic model of the intense laser-cluster interaction in which the laser field is treated self-consistently. We find that for clusters initially as small as ~ 25 Å in radius nonuniform expansion of the heated material results in long-time resonance of the laser field at the critical density plasma layer. A significant result of this is that the ponderomotive force, which is enhanced at the critical density surface, can be large enough to strongly modify the plasma hydrodynamics, even at laser intensities as low as 10^{15} W/cm² for 800 nm laser pulses. Simulations of our recent experiments in extreme ultraviolet and x-ray generation from clusters explain the dependence of generation efficiency on laser pulse width.

DOI: 10.1103/PhysRevE.64.056402

PACS number(s): 52.38.-r, 36.40.Vz

I. INTRODUCTION

The hot dense plasma created by the irradiation of atomic clusters by short, intense laser pulses is a promising, compact source of x rays for applications including next generation extreme ultraviolet (EUV) lithography [1], EUV and x-ray microscopy [2], and x-ray tomography [3]. Recently, nuclear fusion has been demonstrated using collisions of fast ions produced in the rapid expansion of laser-heated deuterium cluster plasmas [4]. Cluster plasma has been proposed as a means for phase matching in high-harmonic generation [5]. Laser-induced cluster plasma is an interesting system spanning the regimes of laser-solid and laser-gas interaction [6–8].

If a pulsed gas jet is operated with sufficiently high backing pressure and an appropriately shaped nozzle, rapid adiabatic expansion cooling of the flowing gas occurs, and atoms are susceptible to efficient clustering through van der Waals forces [9]. Noble gases such as Kr and Xe can form clusters of as many as 10^6 – 10^7 atoms (up to ~ 1000 Å in diameter). Internally these clusters have the atomic density of a solid, even though the volume average density of the ensemble of clusters is low. In the irradiation of a puff of clusters by an intense laser pulse, the microscopic interaction occurs initially with a locally solid material, which is rapidly turned into dense plasma, so that high-density collisional processes are dominant in the cluster ionization and heating.

In this paper, we describe a self-consistent model of the laser-cluster interaction, in which the time-dependent laser field is coupled to the nonequilibrium time-dependent plasma hydrodynamics of the heated cluster. We find that, even for small clusters, the density profile is nonuniform, so that resonance at the critical density surface $N_e(r) \sim N_{cr}$ plays a dominant role in the laser coupling. We also find that the ponderomotive force at the critical density surface exerted by the self-consistent electric field can significantly alter the plasma hydrodynamics, even for vacuum intensities as low as $\sim 10^{15}$ W/cm².

The most successful model to date for the laser-cluster interaction has been the “nanoplasma” model [10], which has reasonably accounted for the observed levels of ionization [6], the observation of fast electrons and ions [7], and

the apparent resonant behavior in the laser-plasma coupling [7,10]. In this model, the cluster is partially ionized directly by the laser field [11] at early times in the pulse, with subsequent heating and ionization dominated by plasma collisional processes, where laser energy is coupled to an expanding plasma sphere. The model assumes that the radial plasma density profile remains uniform during the expansion (“uniform density model”) so that the dipole moment of the plasma sphere is given by $\mathbf{P} = a^3[(\epsilon - 1)/(\epsilon + 2)]\mathbf{E}$, where a is the sphere radius, \mathbf{E} is the external laser field, and ϵ is the cluster plasma dielectric function. This leads to absorption and scattering resonance when $\epsilon + 2 = 0$, or $N_e/N_{cr} \sim 3$, where N_e is the electron density in the expanded cluster, $N_{cr} = m\omega^2/4\pi e^2$ is the critical density, ω is the laser frequency, and m and e are the electron mass and charge. One of the implications of this model is that there must be a narrow time interval during which this resonance occurs as the cluster plasma expands. This can be shown to be

$$\delta t_{res} \approx \frac{2}{3} \frac{v}{\omega} \left(\frac{N_{e0}}{3N_{cr}} \right)^{1/3} \frac{R}{c_s} \quad (1)$$

for a cluster of initial radius R and electron density N_{e0} , where c_s is the plasma sound speed, and v/ω is the normalized collision frequency at $N_e = 3N_{cr}$. For a typical case of $R = 100$ Å, $c_s = 10^7$ cm/s, $N_{e0} = 2 \times 10^{23}$ cm⁻³, $N_{cr} = 1.8 \times 10^{21}$ cm⁻³ (corresponding to $\lambda_{laser} \sim 800$ nm), and an estimate of $v/\omega \sim 0.03$ [assuming a scaling of $v/\omega \sim 3N_{cr}/N_{e0}(v/\omega)_{solid}$, where $(v/\omega)_{solid} \sim 1$ [12]], we get $\delta t_{res} \sim 6$ fs. For a 600 Å cluster, $\delta t_{res} \sim 40$ fs. These time scales are significantly shorter than indicated by pump-probe and variable pulse width measurements where resonant enhancements of absorption and scattering [13,14] appear to last at least several picoseconds. This discrepancy, which cannot be explained by allowing for typical cluster size distributions [13], suggests that a more detailed model of the laser-cluster interaction is required.

II. HYDRODYNAMIC MODEL

In this paper, the laser-cluster interaction is simulated self-consistently by coupling the equation for the electric near field, $\nabla \cdot (\epsilon \mathbf{E}) = 0$, to a one-dimensional (1D) radial La-

grangian hydrocode. The near field treatment is appropriate for the case where $kR_{\max} \ll 1$, where $k = \omega/c$ is the laser wave number and R_{\max} is the maximum radius of the expanding cluster plasma. This is a good approximation for initial cluster sizes much smaller than a laser wavelength and for times not too late in the cluster expansion. Although the 1D treatment is an idealization used for simplicity and speed of calculation, it provides physical insight and can correspond to experiments under certain conditions, as explained below. The dielectric function of the cluster material is taken to be a Drude model $\varepsilon(r) = 1 + 4\pi N_0 \alpha (1 - N_0 \alpha / 3)^{-1} - \xi + i\xi\nu/\omega$. Here $N_0(r)$ is the density of neutral atoms, α is the atomic polarizability, and $\xi(r) = [1 + \nu^2(r)/\omega^2]^{-1} N_e(r)/N_{cr}$, where $N_e(r)$ is the electron density, ω is the laser frequency, and $\nu(r)$ is the collision frequency. The last is obtained by summing the rates of electron collision with each of the neutral and ion species. The calculation includes field ionization [11], collisional ionization, thermal conduction (both gradient based and flux limited [15]), and a time-dependent collisional-radiative model for the ionization dynamics. Starting with a solid density neutral cluster, at each time step the above equation for the electric near field is solved using the neutral, ion, and electron density profiles and the temperature profile of the previous time step, and the resulting electric field ionizes and heats the plasma, driving the cluster dynamics. Thermal conduction at each Lagrangian grid point is taken to be the lesser of the gradient-based value $|\kappa \partial T_e / \partial r|$, where κ is the thermal conductivity and T_e is the electron temperature, and the flux-limited flow [15]. An ideal gas equation of state is used for the cluster plasma. While this is a reasonable assumption at the high temperatures generated by the laser interaction, it cannot take into account any hot electrons generated in the interaction, which are decoupled from the thermal distribution. A more complete treatment, involving kinetic theory, would be appropriate for cases where the hot electron population is a significant fraction of the total, which could be the case for smaller clusters.

Assuming that the incident (external) electric field is $E_0 \hat{\mathbf{z}}$, where $\hat{\mathbf{z}}$ is the polarization unit vector, the code solves for the self-consistent electric field in spherical coordinates $\mathbf{E} = \hat{\mathbf{r}} \tilde{E}_r(r, \theta) - \hat{\boldsymbol{\theta}} \tilde{E}_\theta(r, \theta)$, where $\tilde{E}_r(r, \theta) = E_r(r) \cos \theta$ and $\tilde{E}_\theta(r, \theta) = E_\theta(r) \sin \theta$, and $\hat{\mathbf{r}}$ and $\hat{\boldsymbol{\theta}}$ are polar unit vectors. Note that in the uniform density model [10] $E_r(r) = E_\theta(r) = \text{const}$, resulting in a uniform \mathbf{E} internal to the cluster plasma, directed along $\hat{\mathbf{z}}$. As will be seen, the cluster plasma density is in general nonuniform so that \mathbf{E} remains a function of θ and r , and therefore *even in the near field regime the plasma dynamics are inherently two dimensional*. Note that in the intermediate ($kR_{\max} \sim 1$) and radiation ($kR_{\max} \gg 1$) regimes the interaction must be treated as a 3D problem, because the front and back of the cluster will then have asymmetric interactions for a given laser beam direction.

Since our idealized calculation constrains the plasma dynamics to be one dimensional, we calculate the field's effect on the cluster by using an effective field $E_{\text{eff}}(r) = \langle \mathbf{E} \cdot \mathbf{E}^* \rangle^{1/2}$, where the angular brackets represent an average over solid angle. That is, field ionization [11] is calculated using $E_{\text{eff}}(r)$, and we substitute E_{eff}^2 for $\mathbf{E} \cdot \mathbf{E}^*$ in expres-

sions for the collisional heating rate per unit volume, $\nu \xi \mathbf{E} \cdot \mathbf{E}^* / 4\pi$, and the ponderomotive force per unit volume, $\mathbf{f}_p = (\varepsilon_r - 1) \nabla \cdot (\mathbf{E} \cdot \mathbf{E}^*) / 4\pi$, where ε_r is the real part of the dielectric function. Therefore, for linearly polarized incident fields, the general results of our 1D calculation should be viewed as qualitative, and useful mainly for providing physical insight. There are two situations, however, where the 1D model corresponds more closely with the dynamics. First, the 1D model is a reasonable approximation, even for linear polarization, in the case of strong resonant coupling, as will be seen below. Second, for the special case of two orthogonal incident beams, one linearly polarized and the other circularly polarized, and with a random phase difference between the beams, it can be shown that the time average electric field magnitude is radially symmetric in the near field limit, and the 1D calculation is appropriate.

III. LIMITS OF THE HYDRODYNAMIC MODEL

As a first step, it is useful to examine the conditions under which the hydrodynamic model, in which the plasma dynamics are driven predominantly by the hydrodynamic pressure and the ponderomotive pressure, is appropriate. Early in the laser pulse, free electrons generated by field ionization and the early stages of the avalanche process can escape from the cluster, leaving a residual positive charge that is insufficient to force a return current. The cluster can then expand in response to electrostatic forces (Coulomb explosion) rather than hydrodynamic forces. The hydrodynamic model can therefore break down for small clusters, which can develop a larger fractional residual charge early in the pulse. A calculation of the fractional electron charge that can escape from the cluster allows a comparison of hydrodynamic to Coulomb forces. An upper bound for the rate of electron escape from the cluster is given by

$$\frac{dn}{dt} = \frac{1}{4} \bar{N}_e 4\pi R_{\max}^2 \int_{v_{\text{esc}}}^{\infty} f(v) v dv, \quad (2)$$

where $n(t)$ is the total number of electrons that have escaped from the cluster, \bar{N}_e is the volume average electron density, $f(v) = 4\pi (m/2\pi kT_e)^{3/2} v^2 \exp(-mv^2/2kT_e)$ is the electron velocity distribution function (taken here to be Maxwellian, and neglecting hot electrons, which will be discussed below), and $v_{\text{esc}} = (2E_{\text{esc}}/m)^{1/2}$ is the escape velocity, where $E_{\text{esc}} = ne^2/R_{\max}$ is the electron kinetic energy required to overcome the electrostatic attraction of the positively charged cluster. Determination of $n(t)$ then allows the calculation of the ratio of average hydrodynamic force per unit volume to the average electrostatic force per unit volume:

$$\eta_F(t) = \int_0^{R_{\max}(t)} dr r^2 \left| \frac{-\partial P(r,t)}{\partial r} \right| \bigg/ \int_0^{R_{\max}(t)} dr r^2 \times \frac{1}{8\pi} \left| \frac{\partial E_{\text{elec}}^2(r,t)}{\partial r} \right|, \quad (3)$$

where $P = N_e kT_e$ is the hydrodynamic pressure, $-\partial P / \partial r$ is the hydrodynamic force per unit volume, $E_{\text{elec}}(r,t)$

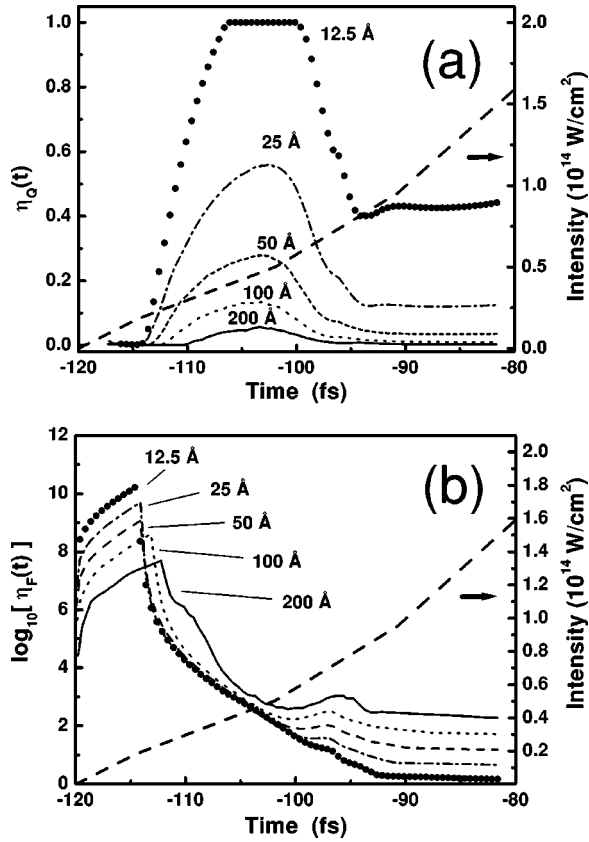


FIG. 1. (a) Cumulative fractional charge $\eta_Q(t)$ escaped from argon cluster during early stages of laser irradiation, for cluster radii 12.5, 25, 50, 100, and 200 Å. Laser: peak intensity 10^{15} W/cm 2 , $\lambda = 800$ nm, 100 fs FWHM Gaussian pulse. Initial cluster atomic density 1.8×10^{22} cm $^{-3}$. Right scale: laser intensity. (b) Logarithm of ratio of average hydrodynamic force density to average Coulomb force density for cluster sizes and laser pulse as in (a).

$= [n(t)e/r^2] \int_0^r dr 4\pi r^2 \rho(r,t) / M$ is the local electrostatic field, and $(1/8\pi) \partial E_{\text{elec}}^2 / \partial r$ is the electrostatic force per unit volume. Here, M is the total cluster mass and ρ is the radial mass density distribution. Because a typical cluster plasma radius is comparable to or smaller than the skin depth of solid density plasma (typically ~ 100 – 200 Å), the residual positive charge density is distributed throughout the cluster volume. It is assumed in the above expression to be distributed according to the ion mass distribution.

For a peak laser intensity of 10^{15} W/cm 2 , $\lambda_{\text{laser}} = 800$ nm, full width at half maximum (FWHM) Gaussian pulse width 100 fs, and initial argon cluster atomic density 1.8×10^{22} cm $^{-3}$, Fig. 1(a) shows the ratio of cumulative escaped charge to the volume integrated electron density,

$$\eta_Q(t) = n(t) / \int_0^{R_{\text{max}}(t)} dr 4\pi r^2 N_e(r,t), \quad (4)$$

as a function of time for a range of initial cluster radii. The rise in $\eta_Q(t)$ between -110 and -105 fs (the laser pulse peak is at $t=0$) corresponds to the rapid increase in electron density as the laser intensity rises through the threshold for field ionization of argon ($\sim 10^{14}$ W/cm 2) [16]. At times, after

~ 100 fs, these electrons seed avalanche ionization, which greatly increases the charge density and therefore $\eta_Q(t)$ decreases owing to the increased electrostatic barrier to escape. Beyond -95 fs, there is little further ionization or electron escape, and $\eta_Q(t)$ saturates. Figure 1(b) shows the corresponding ratio of hydrodynamic force to electrostatic force, from Eq. (3), plotted as $\log_{10}[\eta_F(t)]$. For cluster radii greater than 50 Å, $\eta_F(t)$ is at least 10, and it is at least 100 for 100 Å clusters. For clusters of 25 Å radius and less, η_F decreases to less than 10, and approaches unity for 12.5 Å clusters. Overall, the results shown in Figs. 1(a) and 1(b) indicate that under these conditions the hydrodynamic model is appropriate for clusters as small as ~ 25 Å in radius. Neglecting the influence of hot electrons, higher laser intensities would generate free electrons earlier in the laser pulse envelope, seeding avalanche ionization earlier, resulting in earlier saturation of $\eta_Q(t)$, and increasing the hydrodynamic pressure. Therefore, barring production of a significant fraction of hot electrons, the estimated cluster size limits for the hydrodynamic model are applicable at even higher laser intensities than considered in the calculation of Fig. 1.

IV. COUPLING DYNAMICS

As an example of strong resonant coupling, Fig. 2 shows the results for a 600 Å radius argon cluster of initial atomic density 1.8×10^{22} cm $^{-3}$ irradiated with a linearly polarized 300 fs, 800 nm pulse with peak intensity 1×10^{15} W/cm 2 . These conditions are characteristic of clusters produced in our laboratory for extreme ultraviolet and x-ray generation [17]. The intensity is lower than in our experiments in order to reduce the computation time. Plotted in Fig. 2(a) are electron density profiles and in Fig. 2(b) are corresponding electric field profiles E_{eff} for several times during the pulse envelope. The peak of the pulse occurs at $t=0$. The electric field is scaled relative to its magnitude in vacuum at each time. The field is significantly enhanced with respect to its vacuum value in the region near $N_e \sim N_{\text{cr}}$. There is a persistent resonance at N_{cr} for the full duration of the pulse, arising at early times as a critical density layer expands from the cluster. At very early times ($t < -310$ fs) before plasma is formed it is seen that the relative field amplitude is just less than unity, as expected from dielectric shielding where $\epsilon > 1$. Once plasma develops ($t > -300$ fs), the cluster center is strongly shielded from the electric field, so that the field amplitude there is significantly below its vacuum value. The spatial width of the field resonance at N_{cr} is approximately $\sim [\nu(r_{\text{cr}})/\omega] L_{\text{cr}}$, where $L_{\text{cr}} = |N_e(dN_e/dr)^{-1}|$ is the local scale length at the critical density surface r_{cr} . Since the field resonance width cannot be less than the local Debye length (the Debye length sets the spatial scale for the finest field variations), the effective collision frequency at the critical density surface is clamped to a minimum of λ_D/L_{cr} , where λ_D is the Debye length. In Fig. 2(a), the bump in electron density near the cluster edge at -260 fs is a result of the mass compression driven by the ablative pressure of the expanding material. For these conditions, a weak compression wave propagates to the cluster center as time advances. This effect is present independent of whether the laser pondero-

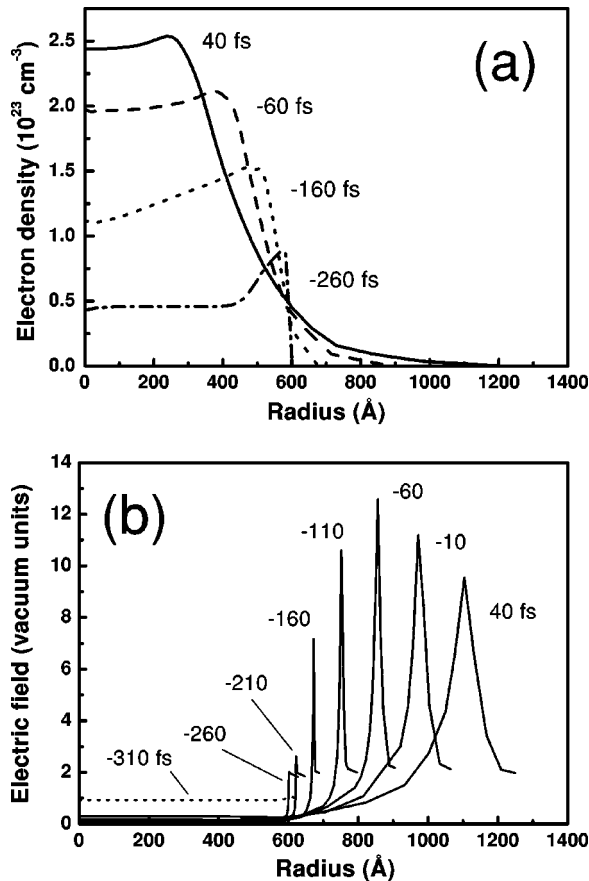


FIG. 2. (a) Electron density profiles vs time for argon cluster of initial radius 600 Å, and laser with peak intensity 10^{15} W/cm², $\lambda = 800$ nm, 300 fs FWHM Gaussian pulse, and initial argon cluster atomic density 1.8×10^{22} cm⁻³. (b) Electric field profiles (normalized to vacuum value) corresponding to the electron density profiles of (a).

motive force is turned on or off. The nonuniform expansion indicated by the electron density profiles is a natural consequence of the expansion of a sphere of hot fluid: at the outside, where the pressure gradient is largest, the fluid velocity is high. In the interior, the pressure gradient is weaker and the radial fluid velocity is reduced. Calculations using a Thomas-Fermi model have shown that nonuniform expansion takes place even for clusters as small as 55 atoms [18].

The coupling resonance at critical density can have a significant radial symmetrizing effect on the field internal to the cluster. This is illustrated by Fig. 3, which shows the ratio $|E_r(r)/E_\theta(r)|$ versus radius at times during the pulse corresponding to the conditions of Fig. 2(b). This ratio peaks at the critical density layer, where it is quite large. For example, at -160 fs, on the rising edge of the pulse, $|E_r(r_{cr})/E_\theta(r_{cr})| \sim 65$ so that $|\tilde{E}_r/\tilde{E}_\theta|^2 \gg 1$ for all θ except for a small band of $\sim 2^\circ$ around the cluster equator (at $\theta = 90^\circ$). From the peak of the pulse to the end, the ratio $|E_r(r_{cr})/E_\theta(r_{cr})|$ remains at least 10, so that outside a 10° band around the equator $|\tilde{E}_r/\tilde{E}_\theta|^2 \gg 1$ at all times. Furthermore, both components \tilde{E}_r and \tilde{E}_θ have large radial gradients only near the critical density surface. Therefore, even though

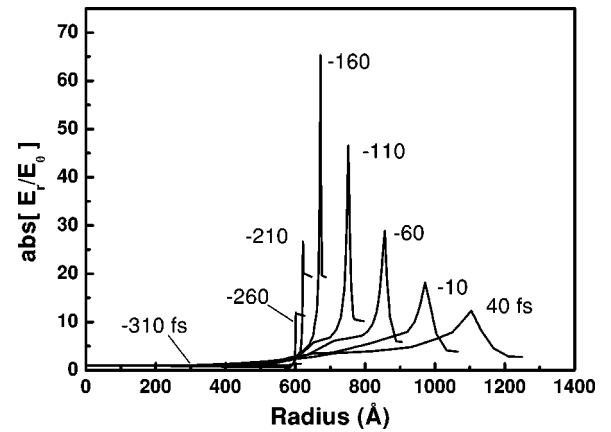


FIG. 3. Absolute value of ratio of radial to tangential field components, showing peak at critical density surface.

the incident laser field is linearly polarized, the effect of the resonance is to promote a predominantly radial ponderomotive force. Under these strong resonant coupling conditions, the radial 1D model comes closer to simulating the actual plasma dynamics.

As a comparison to a previous calculation using the uniform density model [10], we show the results of a simulation for an argon cluster of initial diameter 100 Å, initial atomic density 1.8×10^{22} cm⁻³, laser wavelength 825 nm, pulse width 130 fs, and peak intensity 5×10^{15} W/cm². These are the same parameters used in the calculation of Ref. [10]. Plotted in Fig. 4(a) are electron density profiles and their corresponding electric field profiles for several times during the pulse envelope (the pulse peak is at $t=0$), where the electron density is in units of critical density and the electric field is scaled relative to its magnitude in vacuum. The electric field is enhanced with respect to its vacuum value in the regions of critical density. This promotes significant radial bunching of electron density, attributable to the ponderomotive force. At no point in the cluster plasma evolution does a $3N_{cr}$ resonance appear. Figure 4(b) is a plot of $\log_{10}(N_e^{\max}/N_{cr})$ and central electron temperature T_{e0} for calculations with the ponderomotive force turned on and off, where N_e^{\max} is the value of the largest electron density in the profile. It is seen that a plasma region of critical density or higher is maintained for a longer duration in the case where the ponderomotive force is active. This has the effect of greatly increasing the efficiency and duration of the laser-plasma coupling, as seen in the corresponding temperature plot. Note that the variation of maximum density is similar for the two cases until just past the peak of the pulse, where critical density is approached. Thereafter, the ponderomotive force is quite effective in restraining further expansion. The peak in $\log_{10}(N_e^{\max}/N_{cr})$ near 100 fs is a result of ponderomotive-force-induced compression of the plasma to greater than solid density. While this is a result of our simplification of the problem to a radially symmetric field, it does show the significant effect on the dynamics induced by the ponderomotive force.

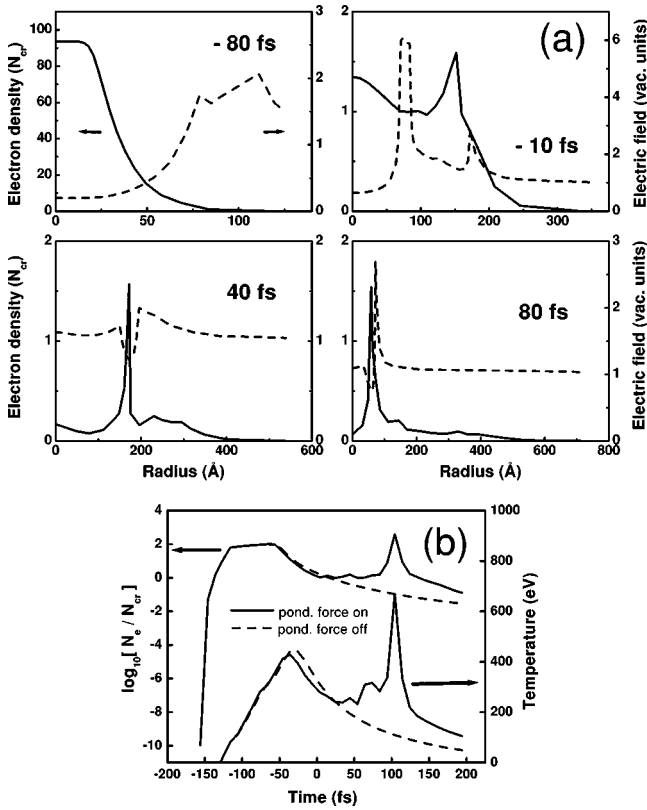


FIG. 4. (a) Electron density profiles (solid lines) and corresponding electric field profiles (dashed lines) at several times for 50 Å argon clusters irradiated by a 5×10^{15} W/cm², $\lambda = 800$ nm, 130 fs FWHM Gaussian pulse. The pulse peak is at $t = 0$. (b) Comparison of cluster plasma peak density and temperature using parameters of (a), with ponderomotive force kept on and turned off.

An important effect not included in the hydrodynamic model, alluded to earlier in the paper, is the generation of hot electrons and their coupling to the cluster plasma. As is well known in cases where resonance absorption takes place, very energetic electrons are produced mostly from the breaking of plasma waves driven by the enhanced electric field at the critical density surface [19]. The overall electron energy distribution of such plasmas is well described by a two-temperature Maxwellian. The lower temperature T_{thermal} , which describes the bulk thermal heating of the plasma, is calculated by our model. The higher temperature is estimated from fits to 2D particle simulations [20] and experiments [21] as $T_{\text{hot}} \text{ (keV)} \sim a(I\lambda^2)^b$, where $a = 3.5$, $b = 0.35$, laser intensity I is in units of 10^{14} W/cm², and wavelength λ is in units of μm . The hot electrons have trajectories from the wave breaking region directly to the plasma core, and away from the plasma and returning, drawn by the resulting space charge force. Stopping power calculations can assess the degree of coupling of these hot electrons to the plasma. An approximate expression [22] for the fraction of hot electron energy transmitted beyond an areal density d (product of electron travel distance and mass density) in solid neutral material is $f(d) = (1 + \eta(d))e^{-\eta(d)}$, where $\eta(d) = 0.59T_{\text{hot}}^{-(1+\mu)/2} \ln(Z/0.3) \sqrt{d/b}$, d is in units of g/cm² and for argon $Z = 18$, $\mu = 0.7$, and $b = 8 \times 10^{-6}$ [22]. This should

be considered a lower limit to the transmission through a hot plasma of the same material and the same integrated areal density. To estimate the fraction of hot electron energy that does not couple to a cluster plasma, we use $d = 2\rho R$, where ρ is the initial mass density of the cluster and R is the initial cluster radius. For an argon cluster with initial radius $R = 600$ Å, $\lambda = 0.8 \mu\text{m}$, and an intensity of 10^{16} W/cm² at the critical density surface (corresponding to less than 10^{15} W/cm² in vacuum—see Fig. 2), we get $f \approx 0.97$. Higher intensities and smaller cluster diameters give values for f even closer to unity. We therefore conclude that for the cluster sizes and intensities examined in this paper hot electrons do not significantly affect the plasma heating. However, as hot electrons can escape from the cluster plasma more readily than thermal electrons, the residual charge left behind may promote electrostatic repulsive forces, especially in small clusters. More sophisticated fluid-based models of the laser-cluster interaction will need to use kinetic theory in order to properly model the hot electrons.

V. ABSORPTION, DISPERSION, AND SCATTERING

The manner in which a laser pulse couples to an individual evolving cluster determines the detailed time dependence of the dielectric function or index of refraction of an ensemble of clusters. This in turn determines the absorption, dispersion, and scattering characteristics of a laser-irradiated cluster jet. These considerations bear directly on practical applications, not only for EUV and x-ray generation [1–3] but also for applications such as the phase matching of high harmonics, which depend on dispersion properties [5]. It is therefore instructive to compare what our calculation predicts for the cluster complex polarizability versus the prediction of the uniform density model [10].

In a radial expansion where the density remains uniform, it can be shown that the plasma velocity profile is necessarily a linear function of radius. Our hydrocode was modified to simulate the uniform density model by forcing the plasma velocity profile to be a linear function of radius. For a 100 Å radius argon cluster heated by a 200 fs FWHM, 800 nm laser pulse at peak intensity 10^{15} W/cm², Figs. 5(a) and 5(b) show $\text{Re}(\gamma)$ and $\text{Im}(\gamma)$ vs time for the uniform density and hydrodynamic models, respectively, where $\mathbf{P} = \gamma \mathbf{E}$ is the dipole moment of the irradiated cluster, \mathbf{E} is the external laser field, and γ is the complex cluster polarizability. Figure 5(c) is a semilogarithmic plot of $\text{Im}(\gamma)$ for both models. The real part of the refractive index of an ensemble of clusters is proportional to $\text{Re}(\gamma)$, while the small signal absorption coefficient is proportional to $\text{Im}(\gamma)$. Determination of \mathbf{P} and γ is made through the dependence $\Phi(\mathbf{r}) = \mathbf{r} \cdot \mathbf{E} + \mathbf{r} \cdot \mathbf{P}/r^3$ (for $r > R_{\text{max}}$) of the near field scalar potential, which is matched to the potential calculated by the code.

For $\text{Re}(\gamma)$, the uniform density model [Fig. 5(a)] shows the classic variation of the dispersion curve through the resonance, which occurs during the cluster expansion as the density decreases through $3N_{\text{cr}}$. Before the resonance is reached, the cluster contributes positively to the refractive index, and negatively afterward. In the hydrodynamic model [Fig. 5(b)], the peak contribution of the cluster to the real

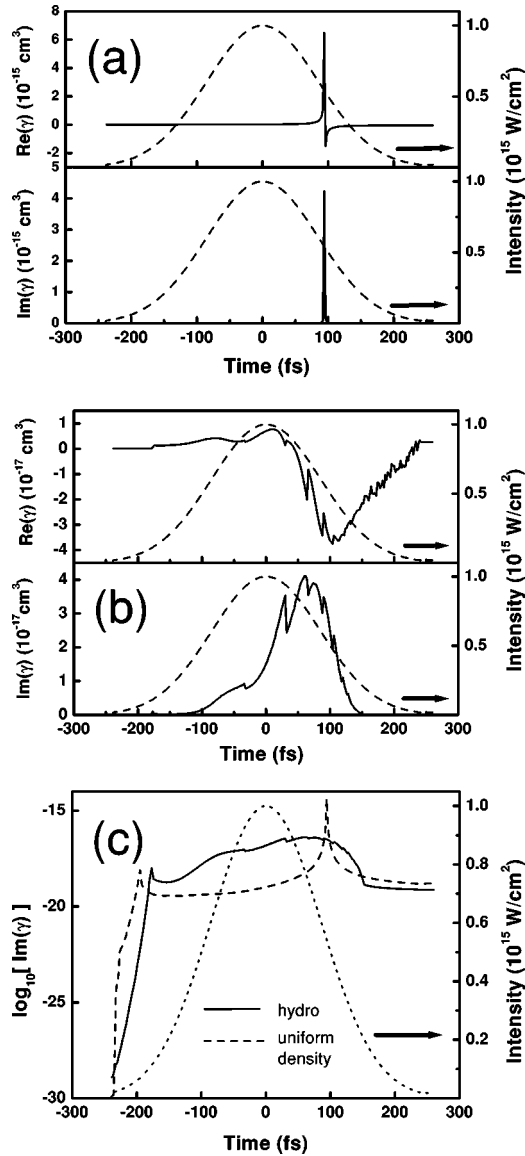


FIG. 5. (a) Real and imaginary parts of the cluster polarizability, calculated using the uniform density model, for an argon cluster of initial radius 100 Å, irradiated by a 10^{15} W/cm 2 , $\lambda = 800$ nm, 200 fs FWHM Gaussian pulse. The laser pulse envelope (right scale) is superimposed as a reference. (b) Real and imaginary parts of the cluster polarizability, calculated using the hydrodynamic model, for the parameters of (a). (c) Logarithm of the imaginary part of the polarizability for both uniform density and hydrodynamic models. At early times both models show a $3N_{\text{cr}}$ resonance.

index is more than ~ 100 times weaker. This is mainly due to the reduced volume of the N_{cr} resonance (at the critical density layer) compared to the full volume $3N_{\text{cr}}$ resonance of the uniform density model. For these particular conditions in the hydrodynamic model, $\text{Im}(\gamma)$ passes through its peak and $\text{Re}(\gamma)$ crosses through zero when the cluster central electron density reaches the nondescript value of $\sim 2.3 \times 10^{22}$ cm $^{-3}$. This point is governed by the value of $(\partial/\partial r)\ln\Phi$ at the plasma-vacuum boundary, and the particular radial density profile in the cluster evolution that gives rise to this point is hard to predict *a priori*.

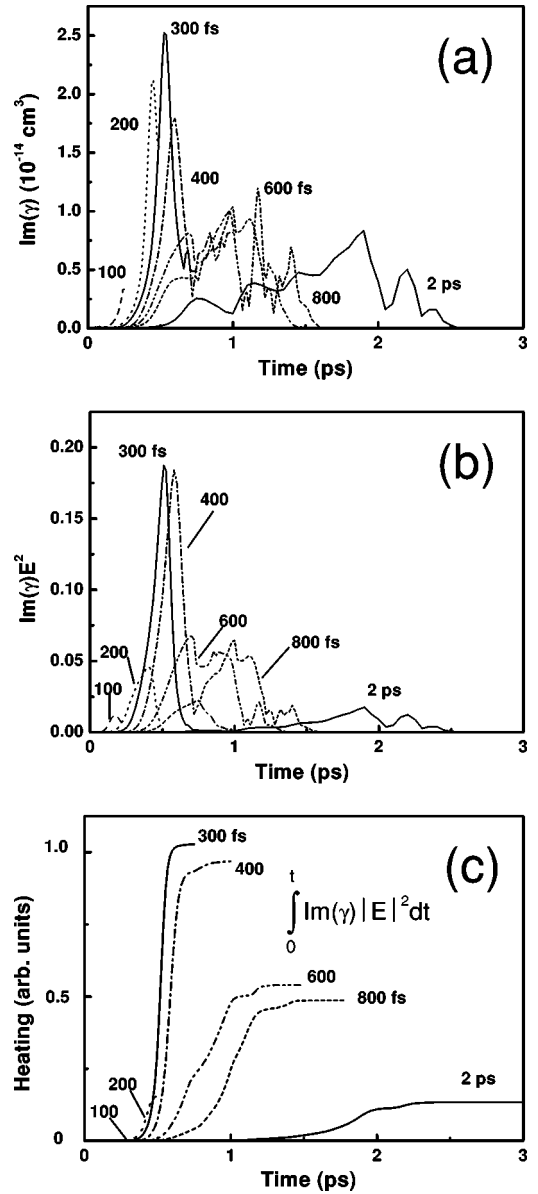


FIG. 6. (a) Imaginary part of argon cluster polarizability vs time for pulsewidths 100, 200, 300, 400, 600, and 800 fs and 2 ps at fixed energy. Cluster initial radius 600 Å. Intensity range 6×10^{15} (100 fs pulses) through 3×10^{14} W/cm 2 (2 ps pulses). (b) Instantaneous heating rate $[\propto \text{Im}(\gamma)|E|^2]$ for laser and cluster conditions as in (a). (c) Cumulative heating $[\propto \int_0^t \text{Im}(\gamma)|E|^2 dt]$ for laser and cluster conditions as in (a).

Examining Fig. 5(c), it is seen that the uniform density model predicts two extremely short-duration intervals of enhanced absorption: one during the rapid ionization in the leading edge of the laser pulse, as the electron density increases through $3N_{\text{cr}}$ on its way up to solid density, and a later interval as the expanding cluster plasma density decreases back through $3N_{\text{cr}}$. The ~ 10 fs duration of the second absorption peak is consistent with the analytic estimate of Eq. (1) for a cluster with $R = 100$ Å. By contrast, the full hydrodynamic model predicts an absorption peak of ~ 100 times less in peak value, but more than 50 times longer in duration. Note that the hydrodynamic model shows that there

is also a very brief $3N_{\text{cr}}$ absorption peak during the rapid ionization early in the laser pulse, before a critical density layer expands from the cluster and the density becomes non-uniform. However, the $3N_{\text{cr}}$ resonance appears at no other time.

The quantity $|\mathbf{P}|^2 = |\gamma|^2 |\mathbf{E}|^2$, which is proportional to the Rayleigh scattered light yield as a function of time, has also been calculated and the duration of enhanced scattering in the uniform density model is similarly about ~ 10 fs, while it is hundreds of femtoseconds in the full hydrodynamic model. The long-time durations of the absorption and scattering results from the full hydrodynamic model are in qualitative agreement with previous experiments [13,14].

In recent experimental work, we examined the efficiency of EUV and x-ray generation from clusters by varying the width of the irradiating laser pulse at fixed laser energy [17]. We found that EUV emission was favored for pulses in the few hundred femtosecond range. Here we simulate this experiment using a 600 \AA radius argon cluster of initial atomic density $1.8 \times 10^{22} \text{ cm}^{-3}$ irradiated with variable width 800 nm pulses in the range 100 fs to 2 ps, with peak intensity varying from 6×10^{15} (100 fs pulse) to $3 \times 10^{14} \text{ W/cm}^2$ (2 ps pulse). The peak intensity is below that in the experiment in order to reduce the computation time, with the goal being a qualitative understanding of the pulse width dependence of cluster heating. For the pulse widths used, Fig. 6(a) shows curves of $\text{Im}(\gamma)$ vs time, Fig. 6(b) shows the instantaneous heating rates $[\propto \text{Im}(\gamma)|\mathbf{E}|^2]$, and Fig. 6(c) shows the cumulative heating $[\propto \int_0^t \text{Im}(\gamma)|\mathbf{E}|^2 dt]$. Although the interaction is highly nonlinear in the laser field, the curves for $\text{Im}(\gamma)$ can be viewed as representing the intrinsic absorbing capabilities of the different pulse width prepared clusters. By this mea-

sure, one would expect the most efficient heating with ~ 300 fs pulses. Including the specific fields to calculate the instantaneous [Fig. 6(b)] and time-integrated [Fig. 6(c)] heating for the various pulses again bears out that ~ 300 fs pulses are most efficient. Detailed examination of the electric field profiles and the electron density profiles shows that the few hundred femtosecond time scale is optimum for resonant absorption: too short a pulse does not allow a significant critical density layer to develop and too long a pulse increases the density scale length sufficiently to reduce the field amplitude penetrating to the critical density surface.

VI. CONCLUSIONS

We have presented a self-consistent 1D model of the intense laser-cluster interaction, where the dominant absorption mechanism is seen to be resonant absorption at the critical density layer. The resonance is maintained throughout the pulse duration as long as the cluster plasma does not expand below critical density. A result of this is that the enhancement of the laser intensity at the critical density surface makes ponderomotive forces an important component of the plasma dynamics. Finally, our recent experiments in EUV and x-ray generation efficiency versus laser pulse width can be explained in terms of the plasma density scale length dependence of resonance absorption.

ACKNOWLEDGMENTS

The authors thank T. Antonsen for useful discussions. This work was supported by the National Science Foundation and the EUV-LLC.

-
- [1] G. D. Kubiak, L. J. Bernardez, K. D. Krenz, D. J. O'Connell, R. Gutowski, and A. M. M. Todd, *OSA Trends Opt. Photonics Ser.* **4**, 66 (1996).
 - [2] J. Kirz, C. Jacobsen, and M. Howells, *Q. Rev. Biophys.* **28**, 33 (1995).
 - [3] Z. H. Levine, A. R. Kalukin, S. P. Frigo, I. McNulty, and M. Kuhn, *Appl. Phys. Lett.* **74**, 150 (1999).
 - [4] T. Ditmire, J. Zweiback, V. P. Yanovsky, T. E. Cowan, G. Hays, and K. B. Wharton, *Nature (London)* **398**, 489 (1999).
 - [5] J. W. G. Tisch, *Phys. Rev. A* **62**, R41802 (2000); T. Tajima, Y. Kishimoto, and M. C. Downer, *Phys. Plasmas* **6**, 3759 (1999).
 - [6] A. McPherson *et al.*, *Phys. Rev. Lett.* **72**, 1810 (1994); *Nature (London)* **370**, 631 (1994).
 - [7] Y. L. Shao *et al.*, *Phys. Rev. Lett.* **77**, 3343 (1996); T. Ditmire *et al.*, *ibid.* **78**, 2732 (1997); *Appl. Phys. Lett.* **71**, 166 (1997); *Phys. Rev. Lett.* **78**, 3121 (1997).
 - [8] M. Lezius *et al.*, *J. Phys. B* **30**, L251 (1997); M. Lezius *et al.*, *Phys. Rev. Lett.* **80**, 261 (1998); S. Dobosz *et al.*, *Phys. Rev. A* **56**, R2526 (1997).
 - [9] O. F. Hagena and W. Obert, *J. Chem. Phys.* **56**, 1793 (1972).
 - [10] T. Ditmire *et al.*, *Phys. Rev. A* **53**, 3379 (1996).
 - [11] M. V. Ammosov, N. B. Delone, and V. P. Krainov, *Zh. Eksp. Teor. Fiz.* **91**, 2008 (1986) [*Sov. Phys. JETP* **64**, 1191 (1987)].
 - [12] H. M. Milchberg *et al.*, *Phys. Rev. Lett.* **61**, 2364 (1988).
 - [13] J. Zweiback, T. Ditmire, and M. D. Perry, *Phys. Rev. A* **59**, R3166 (1999).
 - [14] J. Zweiback, T. Ditmire, and M. D. Perry, *Opt. Express* **6**, 236 (2000).
 - [15] J. P. Matte and J. Virmont, *Phys. Rev. Lett.* **49**, 1936 (1982).
 - [16] S. Augst, D. Strickland, D. D. Meyerhofer, S. L. Chin, and J. H. Eberly, *Phys. Rev. Lett.* **63**, 2212 (1989).
 - [17] E. Parra, I. Alexeev, J. Fan, K. Y. Kim, S. J. McNaught, and H. M. Milchberg, *Phys. Rev. E* **62**, R5931 (2000).
 - [18] M. Rusek, H. Lagadec, and T. Blenski, *Phys. Rev. A* **63**, 013203 (2000).
 - [19] D. W. Forslund, J. M. Kindel, and K. Lee, *Phys. Rev. Lett.* **39**, 284 (1977).
 - [20] K. Estabrook and W. L. Kruer, *Phys. Rev. Lett.* **40**, 42 (1978).
 - [21] D. C. Slater *et al.*, *Phys. Rev. Lett.* **46**, 1199 (1981).
 - [22] R. J. Harrach and R. E. Kidder, *Phys. Rev. A* **23**, 887 (1981).